JACS
JOURNAL OF THE AMERICAN CHEMICAL SOCIETY
Article
pubs.acs.org/JACS

A Generic Approach for the Synthesis of Dimer Nanoclusters and Asymmetric Nanoassemblies

Yongxing Hu and Yugang Sun*

Center for Nanoscale Materials, Argonne National Laboratory, 9700 South Cass Avenue, Argonne, Illinois 60439, United States

Supporting Information

ABSTRACT: Controlled assembly of nanoparticles into asymmetric configurations is of great interest due to their novel properties and promising applications. In this Article, we report a generic strategy for the synthesis of dimer nanoclusters and asymmetric nanoassemblies by using magnetic colloidal substrates, on which tailored surface modification and controlled physical confinement are applied. The modularity of our approach facilitates the fabrication of asymmetric nanostructures with varying sizes, shapes, compositions, surface chemistry, and surface hydrophobicity. Success in the syntheses sheds a light on the versatility of our strategy in rationally designing and synthesizing asymmetric nanostructures with tailored properties and functionalities.

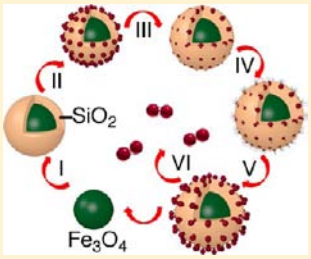

INTRODUCTION

Controlled assembly of nanoparticles into dimers and complex nanoclusters with asymmetric configurations (in terms of geometries and compositions) is of great interest because of their novel properties and possible promising applications (e.g., biosensing, labeling, display, catalysis, etc.).[1] For example, dimers made of either uniform Ag nanoparticles[2] or Au nanoparticles[3] have been demonstrated to be a class of promising surface-enhanced Raman scattering (SERS) substrates due to the creation of hot spots between the individual nanoparticles in each dimer. In these dimers made of equivalent particles (also called homodimers), electromagnetic coupling between the surface plasmon resonances (SPRs) of the individual nanoparticles leads to the enhancement of the optically allowed in-phase mode, while the out-of-phase mode is dark due to the cancellation of the equivalent dipole moments. In contrast, the dimers made of nonequivalent nanoparticles (e.g., Ag/Au nanoparticle heterodimers) enable the observation of both in-phase and out-of-phase modes.[4] In addition to optically active nanoparticles made of noble metals, various nanoparticles can be integrated through controlled assembly to form hybrid nanoclusters with multiple functionalities. Near-field coupling between different components in the nanoclusters may also lead to new properties that cannot be observed in individual nanoparticles.

Some progress has been made in controlled assembly of colloidal nanoparticles into specific clusters.[5] For instance, stability of colloidal Ag nanoparticles capped with poly(vinyl pyrrolidone) (PVP) can be tuned by slightly etching them, leading to spontaneous aggregation of nanoparticles into dimers and clusters.[6] Similarly, citrate-stabilized Au nanoparticles can also form aggregated clusters upon addition of HCl to the nanoparticle dispersions to reduce stability of the Au nanoparticles.[7] Amphiphilic Au nanoparticles capped with both hydrophilic and hydrophobic polymers can be driven to assemble into dimers by tuning the hydrophobicity of solvents.[3a,8] Because of the absence of specific chemical bonding between the individual nanoparticles in the aggregated clusters, additional encapsulation with amorphous shells (e.g., SiO_2, polymer) is usually necessary to fix the clusters.[7,9] An alternative approach to increase the stability of the assembled clusters relies on the modification of the nanoparticle surfaces with linker molecules that can bind nanoparticles together. In the pioneering work demonstrated by Alivisatos and Mirkin, DNA-modified Au nanoparticles can assemble into dimers, trimers, and larger structures through the specific hybridization of the complementary single-stranded DNA molecule.[11] More controllable assembly of Au nanoparticles into clusters has been advanced by Gang and co-workers.[10a] Novak and Feldheim have assembled Au nanoparticles into clusters of dimers, trimers, and tetramers with the use of rigid thiol-functionalized phenylacetylenes as molecular links and templates.[10b] However, it is difficult to synthesize specific clusters with high purity and yield through this approach. In addition, the Au nanoparticle surfaces are passivated by the complete coverage of linker molecules through the strong bonding (i.e., S−Au covalent bonds). Such surface passivation limits the deposition of other interesting molecules on the Au nanoparticles for further applications such as sensing. The rigidity of the linker molecules required by this kind of assembly prevents the possibility to achieve very small interparticle spacing (e.g., <1 nm) due to the large sizes of the linker molecules.

An attractive solution is to selectively decorate the partial surface of a source nanoparticle with synthetic organic or biological molecules, forming "binding patches" that can specifically bond with other nanoparticles. The rest of the unmodified surface on the source nanoparticle is still active for further deposition of interesting species. To create asymmetric chemistries on the surface of a source nanoparticle, the surface

Received: September 25, 2012
Published: January 24, 2013

   dx.doi.org/10.1021/ja309501s | J. Am. Chem. Soc. 2013, 135, 2213−2221

of the nanoparticle has to be partially hidden when it is exposed to linker molecules. One straightforward approach is to deposit nanoparticles on a solid substrate.[12] The physical contacts between the nanoparticles and the substrate prevent the linker molecules from modifying the contact surfaces, leading to the formation of "binding patches" only on the exposed surface regions. Redispersing the patched nanoparticles in appropriate solvents and mixing with other nanoparticles facilitates the assembly of them into dimers or high-level clusters with improved yield and purity.[12,14] Nevertheless, the ratio of surface patches is difficult to tune.[13] The scalability of this method is also limited by the surface areas of the solid substrates used in the syntheses.

In this Article, we report the use of colloidal magnetic Fe_3O_4/SiO_2 core/shell particles as the "solid substrates" together with a controlled physical confinement to assist the asymmetric modification of Au nanoparticle surfaces. The key is the capability that Au nanoparticles anchored on the core/shell particles can be embedded in an additionally deposited SiO_2 layer with controlled surface ratios exposed to linker molecules. The thickness of the additional SiO_2 layer can be well tuned at nanometer scale, indicating the ratio of different surface patches on the Au nanoparticles can be precisely tuned. Moreover, the core/shell particles with submicrometer dimensions exhibit much larger surface areas than do the conventional solid substrates for modification of Au nanoparticles.[13b,14] The good dispersity of Fe_3O_4/SiO_2 core/shell particles in appropriate solvent guarantees the scalable solution-phase synthesis. Besides, the superparamagnetic property of the Fe_3O_4/SiO_2 particles facilitates the efficient purification of products with assistance of an external magnetic field. In addition, small molecules (e.g., cysteamine) can be employed as linkers in our method to create nanoparticle assemblies with very small interparticle spacing (<1 nm). Nanoparticles made of different materials can also be linked to form hybrid asymmetric assemblies. The controllability at the nanometer precision of this method allows one to synthesize complex asymmetric nanostructures in a rational and controllable manner.

EXPERIMENTAL SECTION

Chemicals. Ethanol (denatured), isopropanol (99.9%), hexanes, tetrahydrofunan (THF), ammonium hydroxide aqueous solution (28%), and sodium hydroxide (NaOH, Certified, A.C.S. grade) were purchased from Fisher Scientific. 3-Aminopropyl-triethoxysilane (APTS, 99%) and poly(vinyl pyrrolidone) (PVP) K12 ($M_w \approx 3500$) were obtained from Acros Organics. Poly (acrylic acid) (PAA, $M_w \approx 1800$), tetraethyl orthosilicate (TEOS, 98%), hydrogen tetrachloroaurate (III) trihydrate ($HAuCl_4 \cdot 3H_2O$, 99.9+%), sodium citrate tribasic dihydrate (99%), L-ascorbic acid, silver nitrate ($AgNO_3$, ≥99.0%), cysteamine (~95%), 9-mercapto-1-nonanol, diethylene glycol (DEG), and pentaerythritol tetrakis(2-mercaptoacetate) were obtained from Sigma-Aldrich. PVP K15 ($M_w \approx 10\,000$) was purchased from Fluka. All chemicals were used as received without further purification and treatment.

Synthesis of Fe_3O_4/SiO_2 Core/Shell Colloidal Particles. Fe_3O_4/SiO_2 core/shell colloidal particles were synthesized via the process reported elsewhere.[15] Fe_3O_4 submicrometer particles were prepared through the hydrolysis and reduction of $FeCl_3$ in hot DEG containing NaOH.[16] The synthesized Fe_3O_4 particles were then coated with silica shells through a modified Stöber process. In a typical coating process, ethanol (20 mL) was first mixed with an aqueous dispersion of Fe_3O_4 particles (3 mL, ~7 mg/mL). In the next step, an aqueous solution of ammonium hydroxide (1 mL, 28%) and 0.1 mL of TEOS were added to the Fe_3O_4 particle dispersion to initiate the deposition of silica shells on the Fe_3O_4 particles. This process was performed at room temperature, and mechanical stirring was maintained throughout the whole process. Reaction for 20 min resulted in the formation of silica shells with a thickness of ~16 nm. The Fe_3O_4/SiO_2 core/shell particles were then washed with ethanol two times and redispersed in appropriate solvents to be used as the colloidal substrates for assembling asymmetric nanostructures.

Decoration of Fe_3O_4/SiO_2 Core/Shell Particles with Au Nanoparticles. The Fe_3O_4/SiO_2 core/shell colloidal particles were redispersed in isopropanol (20 mL) containing APTS (50 μL). The outer surfaces of the silica shells were grafted with amino groups after heating the particles at 80 °C for 2 h.[17] The modified particles were then washed with isopropanol twice and redispersed in deionized (DI) water (3 mL). Incubating the modified particles (1.5 mL, 4.2×10^{-4} M) with citrate-stabilized Au nanoparticles (~15 nm in size)[18] under strong sonication led to the adsorption of Au nanoparticles on the Fe_3O_4/SiO_2 core/shell particles. The Fe_3O_4/SiO_2 core/shell particles decorated with Au nanoparticles were separated from the free-standing Au nanoparticles with a magnet, and they were then redispersed in DI water (1 mL) for further use.

Controlled Embedding of Au Nanoparticles with SiO_2 on the Fe_3O_4/SiO_2 Core/Shell Particles. A secondary SiO_2 layer with an appropriate thickness was deposited on the Fe_3O_4/SiO_2 core/shell particles decorated with Au nanoparticles through a Stöber method. In detail, the dispersion (1 mL) of the Fe_3O_4/SiO_2 core/shell particles decorated with Au nanoparticles was mixed with an aqueous solution of PVP K15 (20 mL, 0.02 g/mL) under sonication for 15 min. Applying an external magnetic field separated these particles from the extra PVP molecules in the solution. After being rinsed with DI water, the particles were then redispersed with a solution containing ethanol (20 mL), DI water (3 mL), and ammonium hydroxide aqueous solution (1 mL, 28%). Injection of TEOS (30 μL) to the particle dispersion resulted in the growth of a secondary silica layer only on the SiO_2 shell surface but not on the Au nanoparticles. By adjusting the amount of TEOS, different percentages of the surfaces of the Au nanoparticles can be embedded. The products were then washed with water and redispersed in water (3 mL).

Synthesis of Au Dimer Nanoclusters and Core–Satellite Nanoassemblies. In the Fe_3O_4/SiO_2–Au composite particles synthesized in the previous step, the Au nanoparticles expose a very tiny fraction of surfaces to a solution of cysteamine (0.5 mL, 0.06 g/mL). This exposure led to the graft of cysteamine to the expose Au surfaces to serve as linkers after incubation for 40 min at room temperature. The modified composite particles were purified under a magnetic field and washed with DI water three times to get rid of extra cysteamine molecules in the solution. The resulting composite particles were redispersed in 1 mL of DI water. In the following step, Au nanoparticles with different sizes and different shapes can be added to the dispersion of the modified composite particles for the synthesis of Au dimers. For example, addition of a solution of Au nanoparticles (2 mL, ~15 nm) followed by vortexing for 10 min and incubation for 1 h led to the attachment of the free Au nanoparticles to the cysteamine modified Au surfaces. The final composite particles were then separated by a magnet, washed with DI water twice, and redispersed in an aqueous NaOH solution (4 mL, 0.05 g/mL). Dissolution of SiO_2 in NaOH solution released the Au nanoparticle dimers from the composite particles. The Fe_3O_4 particles were concentrated with a magnet and recycled for a new synthesis. The basic strategy for the synthesis of Au core–satellite asymmetric nanoassemblies follows the synthesis of Au nanoparticle dimers except that Au nanoparticles were embedded with different percentages of surfaces in the secondary SiO_2 layer and Au nanoparticles with much smaller sizes (e.g., ~3 nm)[19] were used to bond with cysteamine linkers.

Synthesis of Asymmetric Dimers Made of Au and Ag Nanoparticles. The process was slightly different from the synthesis of Au dimers. Pentaerythritol tetrakis(2-mercaptoacetate) was chosen as the linker molecule to bridge the exposed Au surface to free Ag nanoparticles in solution. The Ag nanoparticles were synthesized through the Turkevich method, and their surfaces are capped with citrate.[20] Typically, pentaerythritol tetrakis(2-mercaptoacetate) (0.02

mL) dissolved in THF (1 mL) was incubated with the dispersion of the Fe_3O_4/SiO_2 core/shell particles decorated with Au nanoparticles (0.5 mL) at room temperature for 40 min. Extra pentaerythritol tetrakis(2-mercaptoacetate) molecules then were removed by magnetic separation, and the modified composite particles were washed with THF and DI water three times. The resulting particles were redispersed in 1 mL of DI water. In the next step, Ag nanoparticles (2 mL, 0.2 mM) were added to the dispersion of the modified composite particles under sonication. Incubation of the mixture for 1 h ensured the attachment of Ag nanoparticles onto the thiol-grafted Au surface. The composite particles were purified by magnetic separation, washed with DI water twice, and redispersed in aqueous NaOH solution (4 mL, 0.05 g/mL). After the dissolution of SiO_2 with NaOH, the Au–Ag dimers were released from the composite particles.

Synthesis of Amphiphilic Asymmetric Nanoassemblies. After the secondary SiO_2 layer is deposited on the Fe_3O_4/SiO_2 core/shell particles decorated with Au nanoparticles, the exposed surfaces of the Au nanoparticles were first grafted with hydrophobic thiol molecules and then hydrophobic nanoparticles were allowed to assemble on the modified surfaces. Typically, an aqueous dispersion of the Fe_3O_4/SiO_2 core/shell particles decorated with Au nanoparticles (0.5 mL) was transferred to THF (0.5 mL). Adding 9-mercapto-1-nonanol molecules (0.05 mL) to the particle dispersion allowed one to conjugate the thiol molecules on the exposed surface of Au nanoparticles after incubation for 40 min. The resulting composite particles were separated by a magnet, washed with THF three times, and redispersed in THF (0.5 mL). In the next step, hydrophobic nanoparticles dissolved in hexane (such as $Fe@Fe_3O_4$ core/shell nanoparticles or Au nanoparticles (0.02 mL))[21] were added to the THF dispersion of the modified composite particles under strong sonication. The mixtures were dried in air and washed with THF three times. Finally, the composite particles were dispersed in an aqueous NaOH solution (4 mL, 0.05 g/mL) to dissolve the silica layer, leaving amphiphilic asymmetric nanoassemblies in solution.

Characterization. A JEOL 2010F(s) transmission electron microscope was used to characterize the morphology of the particles formed at each step. The as-synthesized particles were dispersed in DI water to form dispersions at appropriate concentrations. To prepare a TEM sample, a drop of particle dispersion was delivered to a carbon-coated copper grid with the use of pipet, followed by evaporation of solvent in air at room temperature. The TEM images were obtained at 200-kV operation voltage. Energy dispersive X-ray spectra (EDS) were collected with an INCA X-ray microanalysis system equipped on JEOL 2010F(s) transmission electron microscope. A JSM JEOL 7500F field-emission scanning electron microscope operated at 10 kV under high-vacuum mode was used to record the SEM images. A VARIAN CARY-50 spectrophotometer was used to record the UV–vis–NIR spectra of the particle dispersions.

RESULTS AND DISCUSSION

Synthesis of Dimers Made of Equivalent Au Nanoparticles. Figure 1 schematically highlights the major steps involved in the formation of "binding patches" on Au nanoparticles and the assembly of them into dimers. The approach starts with the synthesis of superparamagnetic Fe_3O_4 colloidal particles through a high temperature hydrolysis and reduction of $FeCl_3$ in diethylene glycol as reported elsewhere.[16] The Fe_3O_4 particles are then coated with an amorphous SiO_2 layer through a modified Stöber reaction that involves the hydrolysis of tetraethylorthosilicate (TEOS) (step I).[15] Later, the resulting Fe_3O_4/SiO_2 core/shell particles are modified with 3-aminopropyl-triethoxysilane (APTS) in an isopropanol solution to render the particle surfaces with amino groups ($-NH_2$). Mixing the modified core/shell particles with citrate-stabilized Au nanoparticles leads to the graft of Au nanoparticles on the surfaces of Fe_3O_4/SiO_2 core/shell particles due to the strong chemical bonding between Au atoms and N

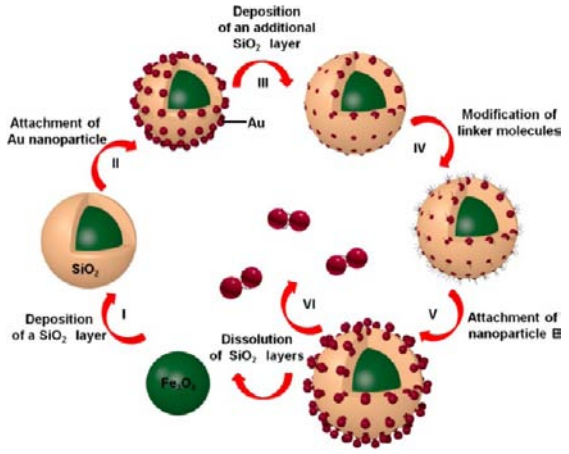

Figure 1. Scheme illustration of the major steps involved in the synthesis of dimers made of Au nanoparticles. Au nanoparticles are first anchored on the surface of Fe_3O_4–SiO_2 core–shell colloidal substrates (II) followed by a physical confinement with a secondary SiO_2 layer (III), leaving the Au nanoparticle surfaces with designed ratio exposed. Selective surface modification is conducted with the addition of linker molecules (IV), followed by the attachment of additional Au nanoparticles (i.e., nanoparticle B) onto the exposed Au surface (V). Free-standing Au nanoparticle dimers are obtained with the removal of SiO_2 layer (VI), and the superparamagnetic Fe_3O_4 cores can be recycled for further synthesis.

atoms in the amino groups (step II). Excessive Au nanoparticles can be easily separated from the composite particles by placing the dispersion in a magnetic field. Because of the significant difference in surface chemistry between Au and SiO_2, repeating the Stöber reaction selectively deposits an additional SiO_2 layer only on the SiO_2 shells rather than Au surfaces, resulting in the partial embedding of the Au nanoparticles in SiO_2 matrix (step III).[17] In general, forming a silica coating on a solid surface by sol–gel methods usually requires the surface with a significant chemical/electrostatic affinity for silica. Citrate-coated Au nanoparticles can be coated with silica after the surfaces of the Au nanoparticles are modified with 3-aminopropyltrimethoxysilane (APTS).[22] However, in our work, surfaces of the Au nanoparticles used in step II are not modified with APTS, and the original citrate coating prevents the direct deposition of silica on the Au nanoparticles in the Stöber reaction. In a control experiment, when both the citrate-stabilized Au nanoparticles and the SiO_2 nanoparticles are exposed to a Stöber reaction solution under the same reaction condition in step III of Figure 1, the resulting SiO_2 only deposits on the SiO_2 nanoparticles. Therefore, when the thickness of this secondary SiO_2 layer is less than the diameter of the Au nanoparticles, the portions of the Au nanoparticle surfaces that are not embedded in the SiO_2 are exposed to the solution environment, accessible by the linker molecules for surface modification in step IV. The thickness of this secondary SiO_2 layer can be precisely tuned at nanometer scale by controlling the reaction conditions, allowing the surfaces of Au nanoparticles to expose at a predefined ratio. In the next step, cysteamine molecules bond to the exposed Au surfaces based on the spontaneous formation of the strong covalent bonds between Au atoms and the –SH groups upon the mixing of an aqueous solution of cysteamine ($HS-CH_2-CH_2-NH_2$) and the dispersion of composite particles (step IV). The dangling amino tails of the cysteamine molecules extrude from the Au nanoparticle surfaces to exhibit adhesive activity toward other

dx.doi.org/10.1021/ja309501s | J. Am. Chem. Soc. 2013, 135, 2213–2221

Au surfaces. As a result, the cysteamine molecules can serve as linkers to bind additional free-standing Au nanoparticles to the Au nanoparticles partially embedded in the SiO_2 matrix (step V). The excessive free-standing Au nanoparticles can be easily removed by applying a magnetic field to selectively concentrate the composite particles. Finally, free-standing dimers made of Au nanoparticles can be collected after the SiO_2 shells are etched by an aqueous solution of NaOH, and the leftover Fe_3O_4 particles are removed with a magnet (VI). The Fe_3O_4 particles can be dispersed and reused in a new synthesis. Involvement of the superparamagnetic Fe_3O_4 particles in the synthesis is crucial for improving yield and purity of the resulting Au nanoparticle dimers because of the high selectivity and efficiency of magnetic separation.

Figure 2 presents electron microscopic images of the particles formed at different stages in the synthesis of dimers made of 15 nm Au nanoparticles. Figure 2a shows a transmission electron microscopy (TEM) image of the composite particles with Au nanoparticles essentially fully buried in SiO_2 matrix (i.e., the product formed after step III of Figure 1). Close observation reveals that the secondary SiO_2 layer deposited in the second Stöber reaction is around 14 nm (Figure 2b), which is very close to the average diameter (i.e., 15 nm) of the embedded Au nanoparticles. Such deep embedding is important for the formation of dimers. Otherwise, undefined agglomerations made of multiple Au nanoparticles are formed when no SiO_2 embedding exists or the SiO_2 embedding is too shallow. The agglomeration of the Au nanoparticles can be ascribed to the detachment of Au nanoparticles from the shallow SiO_2 matrix during surface modification by ligand exchange from citrate to cysteamine. Because of the strong chemical bonding between Au and the −SH groups in cysteamine molecules, the cysteamine molecules may partially penetrate along the interfaces between Au nanoparticles and SiO_2 layers to replace the original citrate ions. The change in surface chemistry from citrate with carboxylate groups to the cysteamine with amino groups lowers the interaction between the surfaces of the Au nanoparticles and the SiO_2 matrix. Figure S1 compares images of the samples with thin secondary SiO_2 layers after cysteamine molecules are introduced, showing the detachment of Au nanoparticles and the formation of agglomerations. If the secondary SiO_2 layer is too thin (e.g., <2 nm for the 15 nm Au nanoparticles), the cysteamine molecules are allowed to penetrate along the Au/SiO_2 interfaces and cover the whole surfaces of the Au nanoparticles, leading to the detachment of Au nanoparticles from the SiO_2 matrix (Figure S1a and b). When the thickness of the secondary SiO_2 layer is increased, the citrate coating on the surfaces of the Au nanoparticles cannot be completely replaced at the interface, and the adhesion force between the Au nanoparticles and the SiO_2 layer is still strong enough to prevent detachment. For instance, when the thickness of secondary SiO_2 layer is ~4 nm, the formation of large agglomerates from detached Au nanoparticles is significantly eliminated (Figure S1c). The deeply embedded Au nanoparticles in Figure 2a clearly show that only a tiny fraction of the surface of individual Au nanoparticles is exposed to the surrounding solution to be modified with cysteamine molecules. Such selective surface modification in combination with the deep embedding provides limited active sites for binding free Au nanoparticles, ruling out the possibility of multiple attachments of Au nanoparticles. The TEM image shown in Figure 2c represents the particles formed after selective surface modification with cysteamine (corresponding to step IV, Figure 1) and graft with free 15 nm Au nanoparticles (corresponding to step V, Figure 1). Figure 2d clearly highlights that only one Au nanoparticle is attached to one embedded Au nanoparticle. The increased density of Au nanoparticles in Figure 2c in comparison with that in Figure 2a demonstrates that additional Au nanoparticles have linked to the Au nanoparticles immobilized on the Fe_3O_4/SiO_2 colloidal substrates. The irregular contrast profiles in TEM images originate from the projection overlaps of multiple Au nanoparticles. The successful linking of free Au nanoparticles to the embedded Au nanoparticles can be further confirmed with SEM images (Figure 2e) that are similar to those of the composite particles formed before the deposition of the secondary SiO_2 layer (i.e., the particles formed after step II, Figure 1) (Supporting Information, Figure S2). The morphological similarity indicates the one-to-one binding between Au nanoparticles. In contrast, the composite particles obtained before the modification with cysteamine have essentially smooth surface (inset, Figure 2e), suggesting that the Au nanoparticles are almost fully embedded in the SiO_2 layer. Only a very small portion of surfaces of the Au nanoparticles is exposed if a close inspection is taken. Moreover, the density of Au nanoparticles in the composite particles shown in Figure 2e is lower than that shown in Figure S2 in the Supporting Information, indicating that some Au nanoparticles are completely buried in the secondarily deposited SiO_2 layer. This result is consistent with the nonuniformity in size (i.e., 15 ± 1.7 nm) of the Au nanoparticles. Only the Au nanoparticles with sizes larger than the thickness (i.e., 14 nm) of the

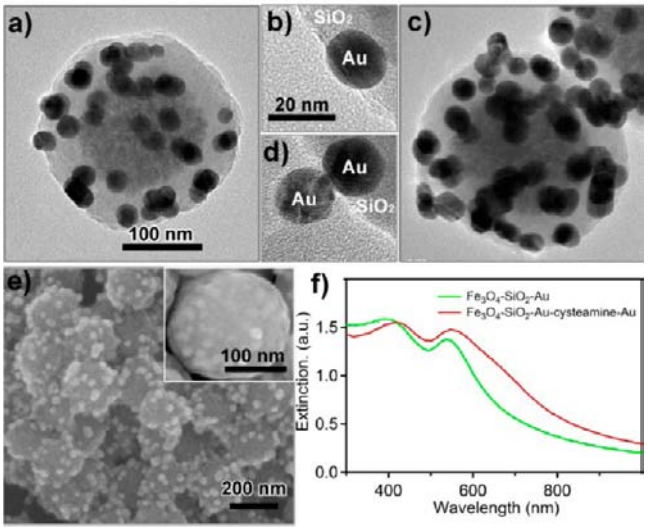

Figure 2. (a) Representative TEM images of Au nanoparticles anchored on the Fe_3O_4/SiO_2 core/shell colloidal substrates. (b) An enlarged TEM image of (a) showing that Au nanoparticles were embedded in the SiO_2 matrix to expose a very small fraction of their surfaces. (c,e) Typical (c) TEM and (e) SEM images of Au nanoparticle dimers anchored on the Fe_3O_4/SiO_2 core/shell particles. Cysteamine molecules were linkers to bind the two individual Au nanoparticles in each dimer. (d) An enlarged TEM image of (c) showing that only one Au nanoparticle was attached to the exposed surface of an embedded Au nanoparticle. (f) Comparison of the UV−vis−NIR extinction spectra obtained from the dispersions of the composite particles shown in (a, green curve) and (c, red curve). Scale bars in (a) and (b) also apply to (c) and (d), respectively.

dx.doi.org/10.1021/ja309501s | J. Am. Chem. Soc. 2013, 135, 2213−2221

secondary SiO_2 layer can partially expose their surfaces, while the Au nanoparticles smaller than 14 nm are completely covered with the secondary SiO_2 layer.

Because of strong SPRs, Au nanoparticles exhibit intensive optical absorption that is influenced by a number of parameters such as the aggregation state between Au nanoparticles.[5b] As a result, dimerization of the Au nanoparticles can be evaluated with the ultraviolet (UV)−visible (vis)−near-infrared (NIR) absorption spectroscopy. The dispersion of the composite particles shown in Figure 2a (i.e., the Fe_3O_4/SiO_2 core/shell particles decorated with Au nanoparticles that are embedded in SiO_2 matrix) displays a light brick red color with broad absorption peaks at 410 and 534 nm, which can be assigned to the absorption of Fe_3O_4 cores and the embedded Au nanoparticles, respectively (green curve, Figure 2f). When additional Au nanoparticles are bonded to the embedded Au nanoparticles to form dimers (as shown in Figure 2c and d), the dispersion of the composite particles undergoes a color change to gray purple corresponding to a red shift of the absorption peaks and an emergence of a broad shoulder in the range of 650−750 nm (red curve, Figure 2f). The shift of the peak from 534 to 550 nm is attributed to the reduced density of conduction electrons in the Au nanoparticles during the ligand exchange of citrate ions with cysteamine molecules in step IV of Figure 1 (see the comparison of spectra in Figure S3, Supporting Information). Because of the stronger chemical bonding formed between cysteamine and the surface Au atoms in the Au nanoparticles than that formed between citrate and the surface Au atoms, more conduction electrons in the Au nanoparticles are immobilized by the cysteamine capping layer, leading to a red shift of the SPR peak of the Au nanoparticles.[23] The appearance of the shoulder peak at longer wavelength is ascribed to the longitudinal SPR mode in the dimers due to the electromagnetic dipole coupling between the two Au nanoparticles in each dimer.[3b]

The dimers consisting of same Au nanoparticles can be released from the colloidal substrates shown in Figure 2c by dissolving SiO_2 with an aqueous solution of NaOH. The Fe_3O_4 cores can be easily removed with the assistance of a magnetic field, leaving a dispersion of pure Au nanoparticle dimers (Figure 3a). Dimers highlighted with red cycles and ellipses represent the dominating structures in the product, although isolated individual Au nanoparticles and clusters made of more than two Au nanoparticles (Supporting Information, Figure S4) are also observed. An enlarged TEM image of a single Au dimer is presented in Figure 3b, clearly showing the surfaces of the Au nanoparticles coated with a thin layer of silicates. The layer of silicates is formed from the concentration of the residual silicates (that are formed from the dissolution of SiO_2 highlighted in step VI, Figure 1) around the dimer surface during the sample drying process. The absence of silicates in the gap between the two Au nanoparticles further proves that the dimers are indeed formed by linker-induced assembly in solution rather than drying-induced assembly. The gap between the Au nanoparticles in each dimer is less than 1 nm corresponding to the size of the linker molecules (i.e., cysteamine). A representative statistical analysis is shown in Figure 3c, revealing the product is composed of 36% single Au nanoparticles, 54% dimers, and 10% of larger clusters with three or more Au nanoparticles. The purity of dimers is comparable to the best results reported in the literature, and it can be further improved by increasing the uniformity of Au nanoparticles in terms of size and morphology. In this work, the Au

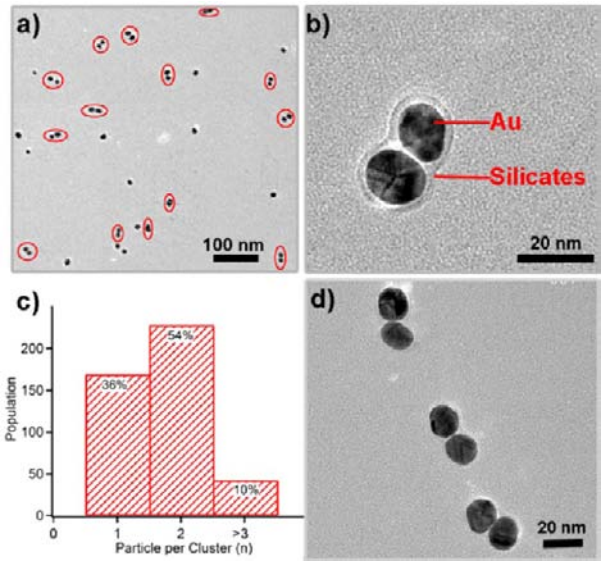

Figure 3. (a) Typical TEM image of free-standing dimers of Au nanoparticles. The dimers are highlighted with red circles and ellipses. (b) An enlarged TEM image of a single dimer coated with silicates after the dimers are dried on the TEM grid. (c) A representative statistical analysis by the histogram, revealing a morphological purity of ~54% dimers, ~36% single particles, and about 10% of nanostructures with three or more Au particles. Overall 432 clusters were analyzed. (d) TEM image of the synthesized Au dimers after they were thoroughly washed with water.

nanoparticles exhibit a size distribution in the range of 13−17 nm. For the Au nanoparticles with sizes smaller than the thickness of the secondary SiO_2 layer (i.e., 14 nm), they are completely embedded in the SiO_2 matrix, preventing them from accessing other Au nanoparticles to from dimers. As a result, these small nanoparticles (with sizes <14 nm) generate the impurity, that is, isolated single nanoparticles, in the product. The clusters made of more than two Au nanoparticles possibly originate from (i) random aggregation of isolated and dimer Au nanoparticles; and (ii) attachment of multiple Au nanoparticles on single large embedded Au nanoparticles during step V of Figure 1. For the Au nanoparticles with size much larger than the thickness of the secondary SiO_2 layer, they can expose surface area large enough to link multiple Au nanoparticles. The residual silicates shown in Figure 3b can be completely removed though a thorough washing with water, resulting in clean dimers as shown in Figure 3d. The dimers are stable in aqueous solution for 4 months, indicating the strong bonding formed between cysteamine molecules and the Au nanoparticles.

Dimers Made of Nonequivalent Au Nanoparticles. In the process shown in Figure 1, the Au nanoparticles used at step II and step V can be independently varied to form asymmetric dimers made of differently sized Au nanoparticles and differently shaped Au nanoparticles. For example, Figure 4a presents a typical TEM image of the asymmetric Au dimers made of Au nanoparticles with size of ~33 and ~15 nm. This sample is synthesized through a process similar to that used for synthesizing the sample shown Figure 3, except that the 33 nm Au nanoparticles are used at step V of Figure 1. The statistic result by analyzing 224 clusters is shown in Figure 4b, revealing that this sample is composed of ~64% dimers, ~32% single particles, and ~4% of clusters with three and more Au particles. The purity of dimers made of two different sized Au

dx.doi.org/10.1021/ja309501s | J. Am. Chem. Soc. 2013, 135, 2213−2221

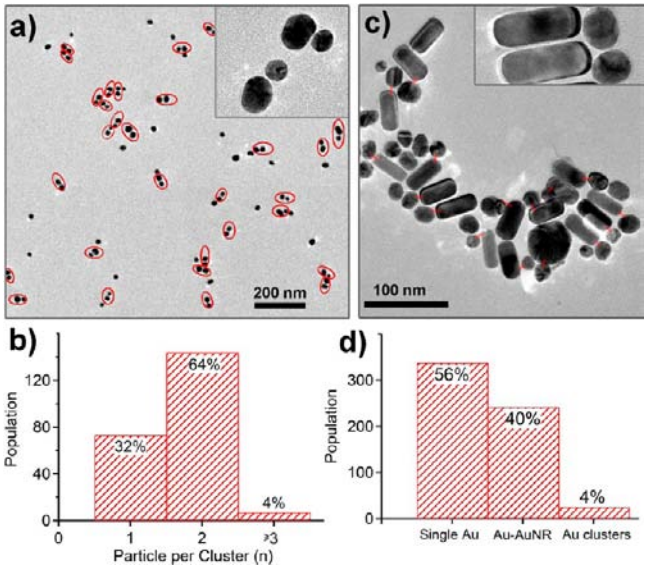

Figure 4. Representative TEM images and statistic analysis of asymmetric dimers made of (a,b) 15 nm Au nanoparticles with 33 nm Au nanoparticles and (c,d) 15 nm Au nanoparticles with Au nanorods. Insets show the corresponding enlarged TEM images of the asymmetric Au nanostructures. The dimers in (a) are highlighted with red ellipses. Each short red line in (c) highlights the linkage between the Au nanoparticle and the Au nanorod in each asymmetric dimer.

nanoparticles is slightly higher than the purity of dimers made of uniformly sized Au nanoparticles shown in Figure 3. The increased purity of dimers can be ascribed to the higher stereohindrance effect from the larger Au nanoparticles with diameter of 33 nm (Figure 4a) in comparison with the 15 nm Au nanoparticles (Figure 3a). The enhanced preference in one-to-one attachment of a single large Au nanoparticle to the expose surface of one Au nanoparticle helps lower the possibility of forming clusters consisting of more than two nanoparticles. Besides the 33 nm Au nanoparticles, addition of Au nanorods to the synthesis solution at step V (Figure 1) facilitates the formation of asymmetric dimers shown in Figure 4c and Figure S5. In most dimers, the Au nanoparticles attach to ends of the Au nanorods rather than the side surfaces of the nanorods, although attachment to the side surfaces of the nanorods is also observed. Such geometric selectivity is ascribed to the difference in activity between the end surfaces and side surfaces in Au nanorods. As for the Au nanorods synthesized with the assistance of cetyl trimethyl ammonium bromide (CTAB), their end surfaces are usually more reactive than their side surfaces.[24] The representative statistical result based on the analysis of 605 clusters is plotted in Figure 4d, showing that this sample is composed of ~40% dimers made of single Au nanoparticles and single Au nanorods, ~56% single particles (including both spherical nanoparticles and nanorods), and ~4% of clusters with three and more Au particles. The purity of nanoparticle–nanorod dimers is lower than that of the dimers made of spherical nanoparticles shown in both Figures 3 and 4a. It is because of the lower concentration of the Au nanorods used, as well as the stronger steric hindrance from the larger Au nanorod dimensions. The CTAB layers on the Au nanorods have to be partially removed through water washing to expose Au surfaces in advance, to enable the formation of bond between cysteamine and the Au nanorods (step V of Figure 1). However, the stability of the Au nanorods in solutions greatly decreases when the CTAB layers are removed. The Au nanorods tend to aggregate when the concentration is high. To avoid aggregation, dispersions of the Au nanorods used for the formation of dimers shown in Figure 4c should be low enough, leading to that many Au nanoparticles are not bonded to Au nanorods. In addition, the Au nanorods have dimensions larger than the spherical Au nanoparticles with sizes of 15 and 33 nm, leading to an enhanced steric hindrance to prevent the attachment of the Au nanorods to the spherical Au nanoparticles. Both reasons are responsible for the increased percentage of single Au spherical nanoparticles in the product. Because the properties of Au nanoparticles are strongly dependent on their physical parameters including size and shape, the examples shown in Figure 4 represent a new class of asymmetric Au dimers for exploiting novel properties originated from the coupling between the two different Au nanoparticles in each dimer.

Compositionally Hybrid Dimers Made of Au Nanoparticles and Ag Nanoparticle. By choosing the appropriate linker molecules at step IV of Figure 1, nanoparticles of different materials can be attached to the Au nanoparticles to form hybrid dimers. For instance, Ag nanoparticles with an average diameter of 11 nm can be attached to the 15 nm Au nanoparticles to form Au–Ag hybrid dimers when tetra-thiol molecules (e.g., pentaerythritol tetrakis(2-mercaptoacetate)) are used as the linkers. Because of the steric hindrance, only a fraction of the thiol groups in pentaerythritol tetrakis(2-mercaptoacetate) molecules can be grafted to the exposed Au surface at step IV of Figure 1. The remaining free thiol groups in the tetra-thiol molecules extend in the solution to bind Ag nanoparticles added at step V of Figure 1, facilitating the generation of hybrid dimers with high purity (Figure 5a).

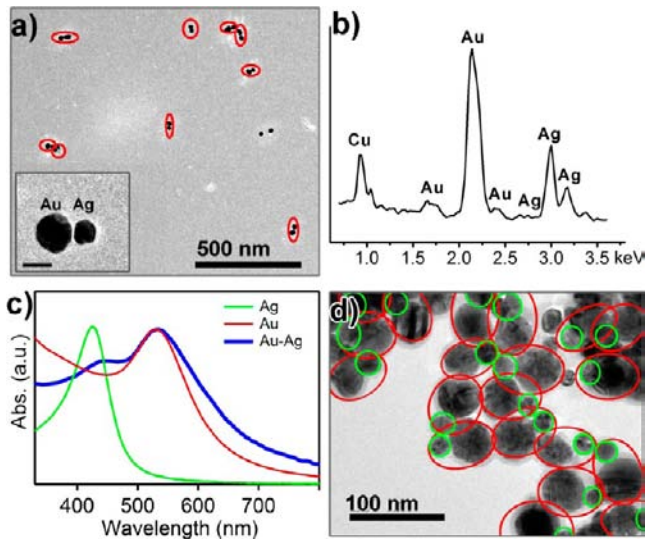

Figure 5. (a) Representative TEM image of the Au–Ag hybrid dimers made of 15 nm Au nanoparticles and 11 nm Ag nanoparticles. The inset highlights an individual Au–Ag dimer, and its scale bar is 15 nm. (b) EDS spectrum of a single Au–Ag dimer, clearly displaying the appearance of both characteristic peaks of Au and Ag. (c) UV–vis–NIR spectra of Au–Ag dimers (blue curve), Au nanoparticles (red curve), and Ag nanoparticles (green curve). (d) Representative TEM image of Au–Ag hybrid dimers made of 15 nm Au nanoparticles and 50 nm Ag nanoparticles. The Au nanoparticles in dimers are highlighted with green circles, while the corresponding dimers are highlighted with red ellipses.

Energy dispersive X-ray spectroscopy (EDS) has been used to confirm the hybrid compositions of the synthesized dimers. As shown in Figure 5b, the EDS spectra of individual dimers are essentially the same and exhibit strong peaks of both Au and Ag, indicating the dimers highlighted in Figure 5a are indeed made of hybrid compositions of Au and Ag. The existence of Cu peaks originates from the TEM Cu grid. Figure 5c compares the optical absorption spectra of the pure Ag nanoparticles (green curve), pure Au nanoparticles (red curve), and the Au–Ag hybrid dimers (blue curve). The Au–Ag dimers exhibit absorption peaks close to the SPR band of both pure Ag and Au nanoparticles, although these peaks red-shift (i.e., from 423 to 440 nm for Ag and from 530 to 535 nm for Au). In addition, the increased broadband absorption in the range of 550–800 nm is due to the electromagnetic dipole coupling between the SPRs of the Au and Ag nanoparticles. The different sizes of the two domains in each dimer help us easily identify that the observed dimers are made of both Au and Ag nanoparticles. However, the size difference is not easily observed in the low-magnification images when the sizes of the Au and Ag nanoparticles are not significantly different. Figure 5d presents a TEM image of Au–Ag heterodimers made of 15 nm Au nanoparticles and 50 nm Ag nanoparticles. More images are shown in Figure S6. Thanks to the significant size difference between the Au and Ag nanoparticles, the heterogeneity of each dimer can be easily determined from the TEM image shown in Figure 5d. In addition, energy-filtered transmission electron microscopy (EFTEM) at the Ag M-edge (450 eV) has been applied to image the distribution of Ag in the dimers. As shown in Figure S7b, the bright areas correspond to Ag and well overlap with the large particles in the bright field TEM image in Figure S7a. The Au nanoparticle domains do not appear in the EFTEM image due to the energy filter, further confirming that the synthesized dimers in Figure 5 are Au–Ag hybrid dimers.

Asymmetric Core–Satellite Nanoassemblies. One advantage of the method shown in Figure 1 is that the percentage of the surfaces of the Au nanoparticles anchored on the Fe_3O_4/SiO_2 core/shell particles can be tuned to expose to solution for modification with linker molecules. The easiest way is to control the Stöber reaction conditions (e.g., reaction time, precursor concentration, etc.) at step III of Figure 1 to tune the thickness of the secondary SiO_2 layer. As a result, novel assembly structures with tunable asymmetries can be achieved by varying the thickness of the secondary SiO_2 layer. For example, multiple free Au nanoparticles with size of ~3 nm can be attached to the exposed surface of a 15 nm Au nanoparticle, generating asymmetric core–satellite assemblies. Figure 6a (and Figure S8) and b (and Figure S9) presents typical TEM images of the core–satellite assemblies made of 15 nm Au nanoparticles as cores and 3 nm Au nanoparticles as satellites, which are prepared with deep and shallow SiO_2 embedding of the 15 nm Au nanoparticles. The enlarged TEM images and the schematic illustrations in Figure 6c clearly demonstrate that the coordination number of 3 nm Au nanoparticles on each 15 nm Au nanoparticle changes according to the depth of 15 nm Au nanoparticle embedded in the SiO_2 matrix. Figure 6d plots the dependence, showing that that larger exposed surface area allows more 3 nm Au nanoparticles to bind on the 15 nm Au nanoparticles. The number of satellites on each asymmetric assembly can be finely tuned by varying the thickness of the secondary layer of SiO_2.

Amphiphilic Janus Au Nanoparticles and the Derived Nanoassemblies. Amphiphilic Au nanoparticles with both hydrophobic and hydrophilic surface regions can also be synthesized by following steps I–IV of Figure 1. At step IV, hydrophobic alkyl thiol molecules (e.g., 9-mercapto-1-nonanol) are used to modify the citrate-capped Au nanoparticles. When the thiol molecules are bonded to the exposed Au surfaces through the strong S–Au bonds, the exposed Au surfaces

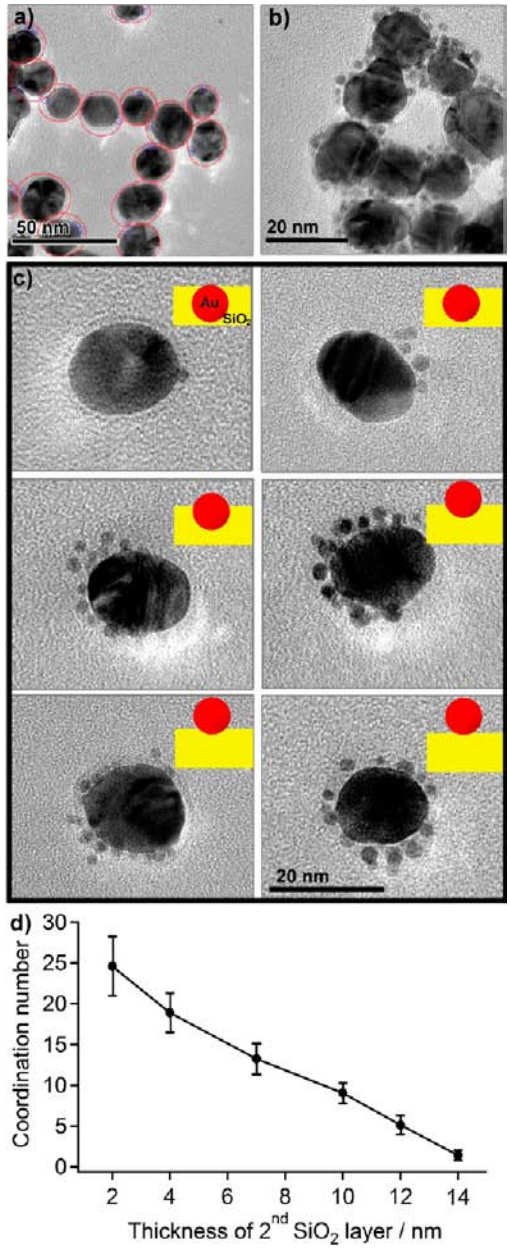

Figure 6. TEM images of Au core–satellite assemblies with varying asymmetries. These assemblies are made of 15 nm Au nanoparticles as cores and 3 nm Au nanoparticles as satellites. Parts (a) and (b) present typical core–satellite assemblies made of 15 nm Au nanoparticles as cores and 3 nm Au nanoparticles as satellites that are prepared with deep and shallow SiO_2 embedding of the 15 nm Au nanoparticles. Each core–satellite assembly in (a) has been highlighted by a pale red circle, while the small satellite (3 nm Au) is highlighted by a blue circle. (c) Enlarged TEM images of the 15 nm Au nanoparticles with gradually more exposed surfaces to bind the 3 nm Au nanoparticles. The insets highlight the percentage of the 15 nm Au nanoparticles' surfaces embedded in the SiO_2 layer. (d) A plot of the dependence between the coordination number of Au (3 nm) to the thickness of the secondary SiO_2 layer based on statistical analysis.

dx.doi.org/10.1021/ja309501s | J. Am. Chem. Soc. 2013, 135, 2213–2221

switch to hydrophobic state due to the long alkyl tails of the thiol molecules. Such modification enables the composite particles to disperse in THF that is a cosolvent for hydrophobic nanoparticles. At step V of Figure 1, variable hydrophobic nanoparticles in hexane are added to the THF dispersion of the composite particles. Drying the mixed dispersion directs the hydrophobic nanoparticles to assemble on the exposed hydrophobic surfaces of the Au nanoparticles due to hydrophobic−hydrophobic interactions. Because hydrophobic−hydrophobic interaction is a long-range force, multiple layers of hydrophobic nanoparticles can be assembled on each Au nanoparticles.[25] Dissolving the SiO_2 exposes the unmodified hydrophilic Au surfaces, resulting in the free-standing amphiphilic nanoassemblies. Figure 7a and b presents the

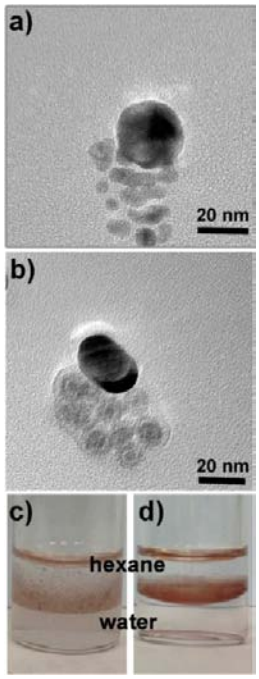

Figure 7. (a,b) Representative TEM images of amphiphilic asymmetric nanoassemblies made of (a) hydrophilic Au nanoparticles (~15 nm) with hydrophobic Au nanoparticles (~4 nm) and (b) hydrophilic Au nanoparticles (~15 nm) with hydrophobic Fe@Fe_3O_4 core/shell nanoparticles. (c,d) Digital photos of the amphiphilic Au−Fe@Fe_3O_4 asymmetric nanoassemblies as shown in (b) dispersed in a mixture of hexane and water: (c) the amphiphilic nanostructures are not well-dispersed either in hexane or in water right after vortex; (d) the amphiphilic nanostructures are stabilized at the interface of hexane/water after the sample has been undisturbed for 40 min.

amphiphilic nanoassemblies obtained with the use of hydrophobic Au nanoparticles (~4 nm in size) and Fe@Fe_3O_4 core/shell nanoparticles, respectively. The amphiphilic feature of the nanoassemblies is further illustrated by the fact that these nanostructures are stable at the interface of water/hexane (Figure 7d). Therefore, our strategy provides a simple route to fabricate novel amphiphilic asymmetric nanostructures with multiple functions that are difficult (or even impossible) to synthesize with conventional methods. The hydrophobic Au nanoparticle shown in Figure 7a exhibits slight aggregation and fusion. These nanoparticles have been synthesized in hexane according to the previously reported approach.[26] When the hydrophobic Au nanoparticles are transferred to THF as described in the Experimental Section, these small Au nanoparticles become unstable due to their large surface energy and incompatible surface chemistry with THF, leading to attachment of different Au nanoparticles followed by slight fusion. In contrast, the hydrophilic Au nanoparticles used in Figure 3 are large in size and have low surface energy. The consistence of aqueous solution during assembly helps the hydrophilic Au nanoparticle remain stable.

■ CONCLUSIONS

In summary, we demonstrated a general strategy for the synthesis of dimer nanoclusters and asymmetric nanoassemblies through a controllable surface modification of Au nanoparticles on superparamagnetic colloidal substrates. The modularity of our approach, based on the abundant choices of linker molecules, enables the integration of nanoparticles with different sizes, shapes, compositions, etc., to form asymmetric nanoassemblies. This strategy can be integrated with other processes, for example, adding a process of seeded-growth of Au nanoparticles at different steps shown in Figure 1, to synthesize asymmetric nanostructures with even higher complexity. Because of the good dispersibility of the Fe_3O_4/SiO_2 core/shell colloidal particles in solutions, they represent a very unique class of recyclable reaction platforms for the possibly scalable synthesis of asymmetric nanostructures with tailored functionalities.

■ ASSOCIATED CONTENT

Ⓢ Supporting Information

TEM images of undefined agglomerations of Au nanoparticles formed when the SiO_2 embedding is shallow and Au clusters as byproduct separated by centrifugation, and SEM image of Fe_3O_4−SiO_2 colloidal substrates decorated with Au nanoparticles. TEM image of Au−Ag (large) hybrid dimers and corresponding energy-filtered transmission electron microscopy (EFTEM) image. This material is available free of charge via the Internet at http://pubs.acs.org.

■ AUTHOR INFORMATION

Corresponding Author

ygsun@anl.gov

Notes

The authors declare no competing financial interest.

■ ACKNOWLEDGMENTS

This work was performed at the Center for Nanoscale Materials, a U.S. Department of Energy, Office of Science, Office of Basic Energy Sciences User Facility under Contract No. DE-AC02-06CH11357. Wes thank Dr. Yuzi Liu and Dr. Sheng Peng for help in TEM characterization and the synthesis of hydrophobic Fe@Fe_3O_4 core/shell nanoparticles and Au nanoparticles.

■ REFERENCES

(1) (a) Lim, D.-K.; Jeon, K.-S.; Kim, H. M.; Nam, J.-M.; Suh, Y. D. *Nat. Mater.* **2010**, *9*, 60. (b) Linic, S.; Christopher, P.; Ingram, D. B. *Nat. Mater.* **2011**, *10*, 911. (c) Halas, N. J.; Lal, S.; Chang, W.-S.; Link, S.; Nordlander, P. *Chem. Rev.* **2011**, *111*, 3913. (d) Fan, J. A.; Wu, C.; Bao, K.; Bao, J.; Bardhan, R.; Halas, N. J.; Manoharan, V. N.; Nordlander, P.; Shvets, G.; Capasso, F. *Science* **2010**, *328*, 1135. (e) Sonnichsen, C.; Reinhard, B. M.; Liphardt, J.; Alivisatos, A. P. *Nat. Biol.* **2005**, *23*, 741. (f) Buck, M. R.; Bondi, J. F.; Schaak, R. E. *Nat. Chem.* **2012**, *4*, 37. (g) Cohen-Hoshen, E.; Bryant, G. W.; Pinkas, I.;

Sperling, J.; Bar-Joseph, I. *Nano Lett.* **2012**, *12*, 4260. (h) Peng, S.; Lei, C.; Ren, Y.; Cook, R. E.; Sun, Y. *Angew. Chem., Int. Ed.* **2011**, *50*, 3158.
(2) Li, W.; Camargo, P. H. C.; Lu, X.; Xia, Y. *Nano Lett.* **2009**, *9*, 485.
(3) (a) Talley, C. E.; Jackson, J. B.; Oubre, C.; Grady, N. K.; Hollars, C. W.; Lane, S. M.; Huser, T. R.; Nordlander, P.; Halas, N. J. *Nano Lett.* **2005**, *5*, 1569. (b) Chen, G.; Wang, Y.; Yang, M.; Xu, J.; Goh, S. J.; Pan, M.; Chen, H. *J. Am. Chem. Soc.* **2010**, *132*, 3644.
(4) Sheikholeslami, S.; Jun, Y.-w.; Jain, P. K.; Alivisatos, A. P. *Nano Lett.* **2010**, *10*, 2655.
(5) (a) Braun, G.; Pavel, I.; Morrill, A. R.; Seferos, D. S.; Bazan, G. C.; Reich, N. O.; Moskovits, M. *J. Am. Chem. Soc.* **2007**, *129*, 7760. (b) Gandra, N.; Abbas, A.; Tian, L.; Singamaneni, S. *Nano Lett.* **2012**, *12*, 2645. (c) Maneeprakorn, W.; Malik, M. A.; O'Brien, P. *J. Am. Chem. Soc.* **2010**, *132*, 1780. (d) Choi, I.; Song, H. D.; Lee, S.; Yang, Y. I.; Kang, T.; Yi, J. *J. Am. Chem. Soc.* **2012**, *134*, 12083.
(6) Li, W.; Camargo, P. H. C.; Au, L.; Zhang, Q.; Rycenga, M.; Xia, Y. *Angew. Chem., Int. Ed.* **2010**, *49*, 164.
(7) Wang, X.; Li, G.; Chen, T.; Yang, M.; Zhang, Z.; Wu, T.; Chen, H. *Nano Lett.* **2008**, *8*, 2643.
(8) Wang, B.; Li, B.; Zhao, B.; Li, C. Y. *J. Am. Chem. Soc.* **2008**, *130*, 11594.
(9) Botella, P.; Corma, A.; Navarro, M. T.; Quesada, M. *J. Mater. Chem.* **2009**, *19*, 3168.
(10) (a) Maye, M. M.; Nykypanchuk, D.; Cuisinier, M.; van der Lelie, D.; Gang, O. *Nat. Mater.* **2009**, *8*, 388. (b) Novak, J. P.; Feldheim, D. L. *J. Am. Chem. Soc.* **2000**, *122*, 3979.
(11) (a) Alivisatos, A. P.; Johnsson, K. P.; Peng, X. G.; Wilson, T. E.; Loweth, C. J.; Bruchez, M. P.; Schultz, P. G. *Nature* **1996**, *382*, 609. (b) Loweth, C. J.; Caldwell, W. B.; Peng, X. G.; Alivisatos, A. P.; Schultz, P. G. *Angew. Chem., Int. Ed.* **1999**, *38*, 1808. (c) Mirkin, C. A.; Letsinger, R. L.; Mucic, R. C.; Storhoff, J. J. *Nature* **1996**, *382*, 607. (d) Nykypanchuk, D.; Maye, M. M.; van der Lelie, D.; Gang, O. *Nature* **2008**, *451*, 549. (e) Park, S. Y.; Lytton-Jean, A. K. R.; Lee, B.; Weigand, S.; Schatz, G. C.; Mirkin, C. A. *Nature* **2008**, *451*, 553.
(12) Kohler, D.; Madaboosi, N.; Delcea, M.; Schmidt, S.; De Geest, B. G.; Volodkin, D. V.; Moehwald, H.; Skirtach, A. G. *Adv. Mater.* **2012**, *24*, 1095.
(13) (a) Wang, Y.; Chen, G.; Yang, M.; Silber, G.; Xing, S.; Tan, L. H.; Wang, B.; Wang, F.; Liu, X.; Li, B.; Chen, H. *Nat. Commun.* **2010**, *1*, 87. (b) Yoon, J. H.; Lim, J.; Yoon, S. *ACS Nano* **2012**, *6*, 7199.
(14) Sardar, R.; Heap, T. B.; Shumaker-Parry, J. S. *J. Am. Chem. Soc.* **2007**, *129*, 5356.
(15) Ge, J.; Yin, Y. *Adv. Mater.* **2008**, *20*, 3485.
(16) Ge, J.; Hu, Y.; Biasini, M.; Beyermann, W.; Yin, Y. *Angew. Chem., Int. Ed.* **2007**, *46*, 4342.
(17) Hu, Y.; Sun, Y. *J. Phys. Chem. C* **2012**, *116*, 13329.
(18) Kimling, J.; Maier, M.; Okenve, B.; Kotaidis, V.; Ballot, H.; Plech, A. *J. Phys. Chem. B* **2006**, *110*, 15700.
(19) Gao, C.; Vuong, J.; Zhang, Q.; Liu, Y.; Yin, Y. *Nanoscale* **2012**, *4*, 2875.
(20) Turkevich, J.; Stevenson, P.; Hillier, J. *Discuss. Faraday Soc.* **1951**, *11*, 55.
(21) (a) Peng, S.; Wang, C.; Xie, J.; Sun, S. *J. Am. Chem. Soc.* **2006**, *128*, 10676. (b) Peng, S.; Lee, Y.; Wang, C.; Yin, H.; Dai, S.; Sun, S. *Nano Res.* **2008**, *1*, 229.
(22) García-Santamaría, F.; Salgueiriño-Maceira, V.; López, C.; Liz-Marzán, L. M. *Langmuir* **2002**, *18*, 4519.
(23) Peng, S.; McMahon, J. M.; Schatz, G. C.; Gray, S. K.; Sun, Y. *Proc. Natl. Acad. Sci. U.S.A.* **2010**, *107*, 14530.
(24) Chen, T.; Du, C.; Tan, L. H.; Shen, Z.; Chen, H. *Nanoscale* **2011**, *3*, 1575.
(25) Israelachvili, J.; Pashley, R. *Nature* **1982**, *300*, 341.
(26) Peng, S.; Lee, Y.; Wang, C.; Yin, H.; Dai, S.; Sun, S. *Nano Res.* **2008**, *1*, 229.